Corticosteroid receptor dynamics : analysis by advanced fluorescence microscopy

Groeneweg, F.L.

Chapter 6

Quantitative analysis of the nuclear dynamics of the Mineralocorticoid Receptor reveals ligand-specific modulation of chromatin binding

Femke L. Groeneweg[1], Martin E. van Royen[2], Rudie Weij[1], Suzanne Fenz[3,4], E. Ron de Kloet[1], Adriaan B. Houtsmuller[2], Thomas S. Schmidt[3], Marcel J.M. Schaaf[5]

Parts of this chapter are published as:

Quantitation of glucocorticoid receptor DNA-binding dynamics by single-molecule microscopy and FRAP. (2014) PlosOne (3):e90532

1 Department of Medical Pharmacology, Leiden University / LUMC, Leiden, The Netherlands.
2 Department of Pathology, Erasmus MC, Rotterdam, The Netherlands.
3 Physics of Life Processes, Institute of Physics, Leiden University, Leiden, The Netherlands.
4 Cell & Developmental Biology, Biocenter, Würzburg University, Würzburg, Germany.
5 Molecular Cell Biology, Institute of Biology, Leiden University, Leiden, The Netherlands.

Steroid receptors are remarkably dynamic within the nucleus where they exert a combination of free diffusion and frequent transient DNA binding events. The frequency and duration of DNA binding is positively correlated to transcriptional potency. Previously we showed that specific interactions between agonist side groups and amino acids within the ligand-binding pocket determine the DNA-binding dynamics of the GR and AR. Here, we study the closely related MR by a combination of single-molecule microscopy and FRAP. This is the first detailed study of the DNA-binding dynamics of the MR. We determined that, when bound to a potent natural agonist, the receptor is bound to chromatin for roughly 50 % of the time in either short ($\sim$0.6 sec, $\sim$30 %) or prolonged (2–3 sec, $\sim$20 %) binding events. This mobility pattern is shifted towards less frequent and shorter DNA-binding events for antagonist-bound MR and, to a lesser extent, when bound to the weak synthetic agonist dexamethasone. We also compared the chromatin binding dynamics of the MR when bound to natural glucocorticoids or mineralocorticoids. Our results show that the two classes of endogenous MR-ligands do not induce different MR-DNA binding dynamics. However, the receptor was less often DNA-bound when activated by the weaker mineralocorticoid DOC, which suggest that specific ligand-receptor interactions do affect the receptors affinity for DNA.

6.1 Introduction

The family of steroid receptors encompasses a large group of related receptors that are present in the nucleus, or translocate to the nucleus upon ligand binding, and act as ligand-induced transcription factors (Fuller, 1991). All family members share key features, but differ largely in ligand specificity, ligand-binding dynamics and in their choice of co-factors, which enables the enormous variety of biological functions that steroid receptors have. In the past decade, imaging studies of fluorescently tagged proteins inside living cells showed that steroid receptors, and transcription factors in general, display a remarkably high mobility in the nucleus (Stenoien et al., 2000, 2001; Stavreva et al., 2004; Schaaf et al., 2005, 2006; Hager et al., 2009; van Royen et al., 2009b, 2014; Mueller et al., 2010). This high mobility is characterized by free diffusion intermitted by frequent, but transient, DNA binding (Gorski et al., 2006; Biddie and Hager, 2009).

We have previously employed a combination of imaging techniques to study the nuclear dynamics of two steroid receptors, the GR and the AR (van Royen et al., 2014). In these studies, we combined SMM and FRAP and, for the AR, also FCS. SMM enables an unbiased quantification of protein dynamics with high temporal and spatial resolution (Semrau and Schmidt, 2007; Lord et al., 2010; Li and Xie, 2011). The combination with FRAP allows cross-validation with an independent analysis method and greatly extends the time line (from 50 ms for SMM to a minute with FRAP), thus enabling quantification of DNA-binding times (Farla et al., 2004; van Royen et al., 2009a). We found that this combination of techniques gave a consistent pattern of both AR and GR nuclear dynamics and identified 3 fractions for each steroid receptor; one diffusing fraction, and two transiently bound fractions, with DNA-binding times of half a second to several seconds (van Royen et al., 2014).

In the current study, we utilize the same combinational approach of SMM supplemented with FRAP to study the nuclear dynamics of a third steroid receptor: the MR. The chromatin binding dynamics of the MR have not been studied extensively (Tirard et al., 2007; Nishi et al., 2011). The receptor shares a high sequence analogy with both the GR and AR (Fagart et al., 1998). It is activated by the naturally occurring glucocorticoids (cortisol or corticosterone) and by mineralocorticoids (aldosterone and DOC) (Arriza et al., 1987; Joëls et al., 2008; Funder, 2010). As such the MR shares part of its endogenous ligands with the GR, but with different affinities. Cortisol and corticosterone have a much higher affinity for the MR than for the GR (Reul and de Kloet, 1985), whereas many synthetic glucocorticoids, such as prednisolone and dexamethasone, have a very high affinity for the GR but only little affinity for the MR (Arriza et al., 1987; Grossmann et al., 2004). Interestingly, for the GR we found that agonist properties determine the receptor's DNA-binding properties in a manner unrelated to receptor-ligand binding dynamics (*Chapter* 5). We propose that ligand-induced effects are due to their specific binding profile within the receptors ligand-binding groove, which ultimately affects the receptor's affinity for DNA (*Chapter* 5). Although the MR and GR share ∼55 % sequence homology

within their LBD, they differ much more in their ligand-binding pocket architecture (Fagart et al., 1998; Li et al., 2005) and a different set of interactions occur between the steroids and the receptor's ligand-binding pocket (Bledsoe et al., 2002, 2005; Huyet et al., 2012). Thus, we expect different steroid side groups to affect binding strength to the MR and thus likely to affect its nuclear mobility.

Here, we report that agonist-bound MR shows three functionally distinct states within the nucleus. MRs spend approximately 50 % of the time diffusing through the nucleus, the remaining time the receptor is transiently bound to chromatin for either short (∼30 %: 0.5–0.8 sec) or longer (∼20 %: 2–3 sec) binding events. When bound to an antagonist, the MR spends more time diffusing (∼70 %), with a moderately higher diffusion coefficient and loses most of its capacity for longer DNA-binding; short DNA-binding is hardly affected. Finally, we find that agonist properties affect MR's nuclear mobility, with a role for the 11-hydroxyl group. No overall difference in MR's nuclear dynamics was found when bound to endogenous glucocorticoids or mineralocorticoids.

6.2 Methods

Cell culture and transfection

For all experiments transiently transfected COS-1 cells were used. Cultures were maintained in high glucose D-MEM, supplemented with 10 % FBS and 1 % Pennicillin/Streptomycin (all Invitrogen). Transfections were performed with the TransIT-COS kit (Mirus), according to the manufacturer's instructions (500 ng DNA / 10 cm^2). Transfected cells were used in experiments 2–5 days after transfection. pEYFP-hMR was generated by PCR amplification (Phusion HF polymerase, Finnzymes) of the human MR gene from a pRSV human MR template (kindly provided by Dr. R. Evans and described in Arriza et al. (1987)). A set of primers was designed to generate BglII and SmaI sites at the 5′ and 3′ end of the MR coding sequence. Subsequently, the PCR fragment was digested with BglII and SmaI, purified and cloned into the pEYFP-C1 vector, resulting in a vector with an in-frame fusion of hMR with EYFP, separated by 17, mostly nonpolar, amino acids. Plasmid integrity was checked by sequencing. YFP-YFP is a fusion product of EYFP with a second non-fluorescent YFP in the original pEYFP-C1 construct.

Confocal microscopy, western blot and luciferase assays

For confocal analysis, COS-1 cells were grown on coverslips and transfected with YFP-MR (500 ng / 10 cm^2). 48 h after transfection cells were fixated with 4 % PFA for 15 minutes and nuclei were stained with 1 µg/ml Hoechst 33258 (Invitrogen) in 0.1 % PBST for 10 minutes and mounted with Aqua Poly/Mount (Polysciences Europe). Confocal images were obtained with a Nikon TE-2000 E confocal microscope equipped with a 60× oil-immersion objective. eYFP expression was analyzed using the 488 excitation laser and emission collected at 510–530 nm. Exposure and gain settings were adjusted as to prevent over or underexposure. Image analysis was performed with ImageJ.

For western blot, COS-1 cells transfected with the required plasmids (500 ng / 10 cm^2) were harvested 48 h after transfection and prepared for western blot. Protein lysates, SDS-polyacrylamide gel electrophoresis and western blotting were performed as described previously (Vreugdenhil et al., 2007). MR protein was detected with 1:1000 MR 1D5 (generous gift of Gomez-Sanchez (Gomez-Sanchez et al., 2006)) and all samples were co-assessed for α-tubulin (1:5000; Sigma-Aldrich) in combination with 1:5000 goat-anti-mouse IgG HRP. All antibodies were diluted in TBST with 0.5 % milk powder. Detection was performed with the ECL detection system (GE Healthcare).

For the luciferase assay, COS-1 cells were transfected with a combination of 500 ng / 10 cm^2 YFP-YFP, YFP-MR or MR together with 100 ng / 10 cm^2 TAT3-Luciferase (tyrosine amino transferase triple hormone response element) and 2 ng / 10 cm^2 pCMV-Renilla (Promega). 24 h after transfection cells were treated with 10 nM corticosterone, 10 nM aldosterone or 0.001 % EtOH in culture medium supplemented with charcoal stripped FBS. After 20 h, cells were lysed with passive lysis buffer and firefly and renilla luciferase luminescence was determined according to the general prescription of the dual label reporter essay (Promega) on a luminometer (CENTRO XS3 LB960, Berthold).

Compounds

The following hormones were used in these studies: aldosterone, corticosterone, cortisol, deoxycorticosterone (*21-hydroxy-4-pregnene-3,20-dione, 4-pregnen-21-ol-3,20-dione*), spironolactone (*4-pregnen-21-oic acid-17α-ol-3-one-7α-thiol γ-lactone 7-acetate, 7α-(acetylthio)-17α-hydroxy-3-oxopregn-4-ene-21-carboxylic acid γ-lactone*), eplerenone (*pregn-4-ene-7,21-dicarboxylic acid, 9,11-epoxy-17-hydroxy-3-oxo-, γ-lactone, methyl ester*) and dexamethasone. All steroids were purchased from Sigma-Aldrich and diluted in 100 % EtOH to a concentration of 1 mM, except for eplerenone, which was diluted in DMSO. Steroids were further diluted to their required concentrations in the respective media.

Single-molecule microscopy

For all SMM experiments, COS-1 cells were grown on coverslips and transiently transfected with YFP-MR (500 ng / 10 cm^2) 3–5 days prior to analysis. Before SMM recordings, cells were exposed to 1 µM of corresponding hormones for 3–6 h. For SMM measurements, this medium was replaced by serum- and phenol red-free D-MEM medium (Invitrogen), which is also supplemented with 1 µM of the corresponding hormone. Subsequently, cells were transferred to the SMM setup and imaged for up to 90 min at 35 °C. A wide-field fluorescence microscope (Axiovert 100TV, Zeiss) was used, equipped with a 100× / 1.4NA oil-immersion objective (Zeiss). A region-of-interest (ROI) of 50 × 50 pixels (pixel size of 220 nm) was selected. The sample was illuminated by an 514 nm argon laser at an intensity of 2 kW/cm^2. The pulse length of 3 ms was controlled by an acusto-optical tunable filter (AA optoelectronics, France). The EYFP fluorescence signal was detected through a combination of filters (DCLP530, HQ570/80 (Chroma Technology, Brattleboro, VT) and OG530-3 (Schott, Mainz, Germany)), by a liquid-nitrogen cooled CCD camera (Princeton Instruments, Trenton, NJ), camera read out and AOTF timing were tightly controlled. Moderately fluorescent nuclei were selected and photobleached until single fluorescence intensity peaks could be distinguished. The position of each individual molecule was fitted with the intensity profile of a 2D Gaussian model of EYFP peaks (Harms et al., 2001). Our peaks were identified with a signal to noise ratio of ∼8 (peak fluorescent intensity divided by the variation of the background),

which resulted in a positional accuracy of $\sim$40 nm in the X- and Y-direction (determined by the quotient of the full-width-at-half-maximum of the Gaussian fit and the square root of the number of photons detected (Bobroff, 1986)). On average, each picture contained $\sim$1.5 peaks. Image sequences were recorded in series of 8 subsequent images with a time lag of either 6.25 ms or 12.5 ms (Figure 6.1B). Data on molecular dynamics were obtained for multiple step sizes. We used all time lags from 6.25 to 37.5 ms in our analysis. From each cell 180 series of 8 images were taken and data from 20 independent cells (imaged on at least 3 different days) was combined for the analysis.

PICS analysis of single-molecule kinetics

We used the Particle Image Correlation Spectroscopy (PICS) method to determine peak displacement over time (Semrau and Schmidt, 2007). PICS procedures are described in detail in *Chapters 4 and 5*. In short, random correlations between unrelated molecules are subtracted from the cumulative cross-correlation between peak positions at two different time lags. This gives a cumulative probability function (P_{cum}) of diffusion steps l. We use population modeling to calculate diffusion characteristics of the nuclear population of YFP-MR molecules and found that a two-population model best describes YFP-MR's dynamics (Figure 6.1C). The two populations are determined with Given that the population of molecules is homogeneous, a single population of displacing molecules is determined with.

$$P_{\text{cum}}(l, \Delta t) = 1 - \left[\alpha \cdot \exp\left(-\frac{l^2}{\text{MSD}_1(\Delta t)}\right)(1-\alpha) \cdot \exp\left(-\frac{l^2}{\text{MSD}_2(\Delta t)}\right)\right] \tag{6.1}$$

Where MSD_1 and MSD_2 denote the mean square displacement of the first (fast) and the second (slow) fractions respectively, and α is the fraction size of the first (fast) fraction. The analysis was repeated for each time lag and α, MSD_1 and MSD_2 were plotted against time (Δt). The displacements over time were best described using a free diffusion model in 2D, from which the diffusion coefficients (D_{fast} and D_{slow}) were calculated using the following equation:

$$\text{MSD}_i(\Delta t) = 4 \cdot D_i \cdot \Delta t \tag{6.2}$$

OriginPro software was used to obtain weighted, linear fits, to calculate D_{fast} and D_{slow}. The fraction size α decreased slightly (on average -0.27 ± 0.07 %/ms) over increasing time lags in all groups. Due to this effect, we always report the fraction distribution of the smallest time step (6.25 ms) as a representative of the overall fraction distribution. All analyses were first performed on all data from each treatment group pooled together ($n = 20$). Subsequently, all analyses were run again in 3 fractions ($n = 6/7$) and these 3 separate analyses are used to generate standard errors of the mean.

FRAP

For FRAP recordings, COS-1 cells were grown on coverslips and transiently transfected with 500 ng / 10 cm^2 YFP-MR and used 2–3 days after transfection. Before FRAP recordings, cells were exposed to 1 µM of the appropriate ligand for 3–6 hours in normal growth medium. For each experiment, a coverglass with transfected COS-1 cells was placed in a preheated ring and medium was replaced for empty D-MEM without phenol red, supplemented with 1 µM of the corresponding ligand. Cells were used for no longer than 90 minutes and kept at 37 °C and 5 % CO_2. We used a Zeiss LSM510 META confocal laser scanning microscope equipped with a

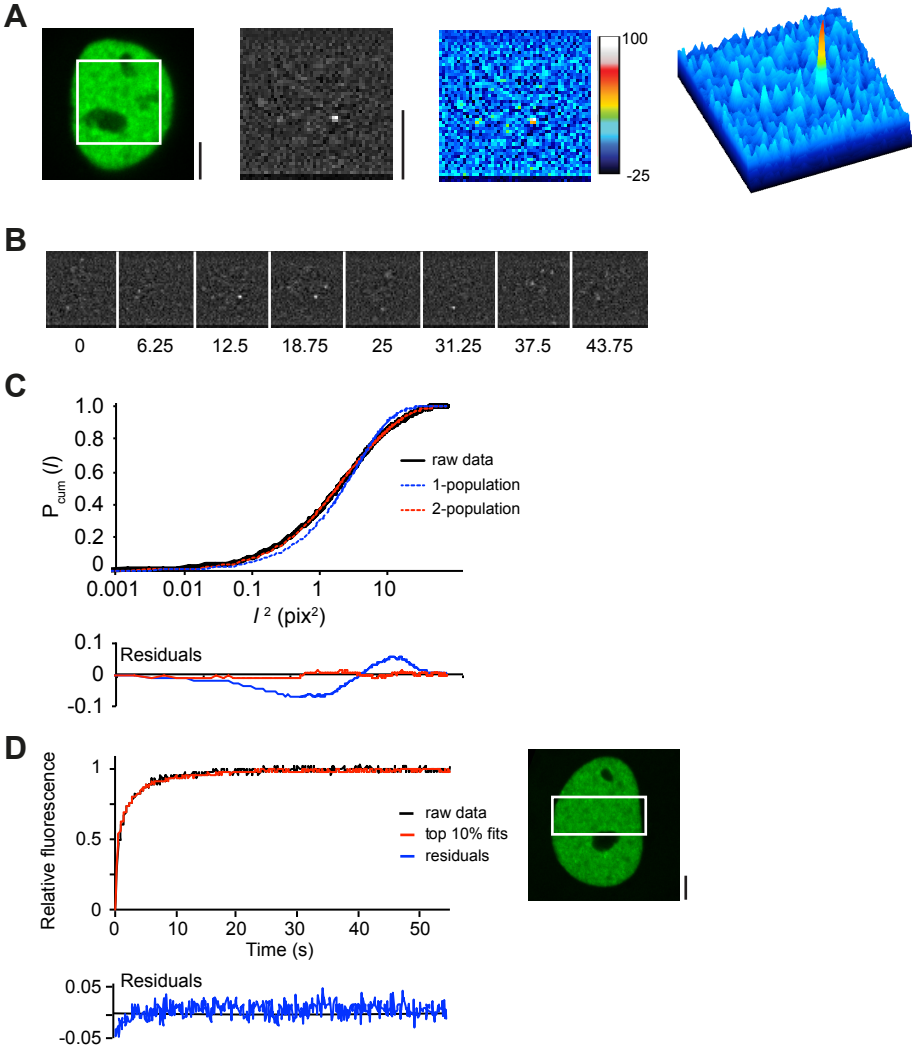

Figure 6.1: SMM and FRAP procedures
(A) A 11 µm × 11 µm area within a nucleus is bleached to obtain single fluorescent peaks representing single YFP molecules. A representative CCD image of single molecules of YFP-MR after background subtraction shows single discernible Gaussian peaks of YFP fluorescence. (B) Regime for single molecule kinetics; images were taken with a time lag of 6.25 ms or 12.5 ms in 300 series of 8 per cell. In background-subtracted images, single molecules of YFP fluorescence are easily discernible. (C) PICS analysis of single molecule displacements, shown for corticosterone-bound YFP-MR at time delay of 6.25 ms. The cumulative probability distribution as a function of the squared distance l^2 (black line) was best fitted with a 2-population model (red line), while a 1-population model gives a suboptimal fit (blue line) ($n = 20$ cells). (D) FRAP procedure of corticosterone-bound YFP-MR. At $t = 0$ s a 100 ms bleach pulse was applied to a strip spanning the nucleus. Subsequently, FRAP recovery curves of 30 cells were recorded, combined and adjusted to baseline fluorescence (black line). Subsequently, Monte Carlo simulations were generated using a 3-population model and fitted to the combined FRAP curve. The top 10 fits were combined (red line) and showed a good fit of the experimental data with small residuals (blue line).

40× / 1.3NA oil-immersion objective, an argon laser (30 mW) and an AOTF. For FRAP analysis a narrow strip spanning the entire width of the nucleus was scanned at 514 nm excitation with short intervals (100 ms) at low laser power (0.2 %). Fluorescence intensity was recorded using a 560 nm longpass filter. After 40 scans, a high intensity (100 % laser power), 100 ms-bleach pulse at 514 nm was applied over the whole strip. Subsequently, the recovery of the fluorescence intensity in the strip was followed for another 55 seconds at 100 ms intervals. For each treatment group 30 cells were measured by FRAP on two separate days. All curves were normalized to baseline fluorescence intensity and combined.

Monte Carlo quantification of FRAP curves

The FRAP data was quantitatively analyzed by comparing the experimental data to curves generated using Monte Carlo modeling (van Royen et al., 2009b). The Monte Carlo simulation is described in detail in *Chapter* 5. In short, simulated FRAP curves were generated with a 3-population model, containing a diffusing fraction and two bound (immobile) fractions. We take the D_{fast} obtained from SMM analysis as a fixed parameter in these simulation, leaving 4 parameters as variables: short bound fraction, long bound fraction (both ranging from 0–90 %), and time spent in short and long bound state (ranging from 0.1 s to 1 s and from 1 s to 300 s respectively). A description of the calculation for all parameters can be found in *Chapter* 5. The laser bleach pulse was simulated based on experimentally derived three-dimensional laser intensity profiles, which were used to determine the probability for each molecule to get bleached considering their 3D position. In all simulations, the size of the ellipsoid was based on the average size of measured nuclei, and the FRAP region used in the measurements determined the size of the simulated bleach region. The laser intensity profile using the simulation of the bleaching step was previously derived from confocal image stacks of chemically fixed nuclei containing GFP that were exposed to a stationary laser beam at various intensities and varying exposure times. The unit time step (Δt) corresponded to the experimental sample rate of 21 ms. The number of molecules in the simulations was 10^6, which was empirically determined by producing curves that closely approximate the data with comparable fluctuations. The parameters of the top 10 best fitting Monte Carlo curves (by ordinary least squares) were averaged to represent the properties of the fractions in the experimental data.

6.3 Results

Characterization of YFP-tagged MR

A fusion of the human MR gene, N-terminally tagged with enhanced YFP, was generated. We assessed if the YFP-tag does not affect the function of the MR. First, we showed that YFP-MR is present throughout the cytoplasm and nucleus when unbound and translocates to the nucleus upon application of a high concentration of ligand (Figure 6.2A). Next, we showed that the YFP-MR fusion protein retains its predicted size by Western blot (27 kDa larger than the untagged MR; Figure 6.2B). No

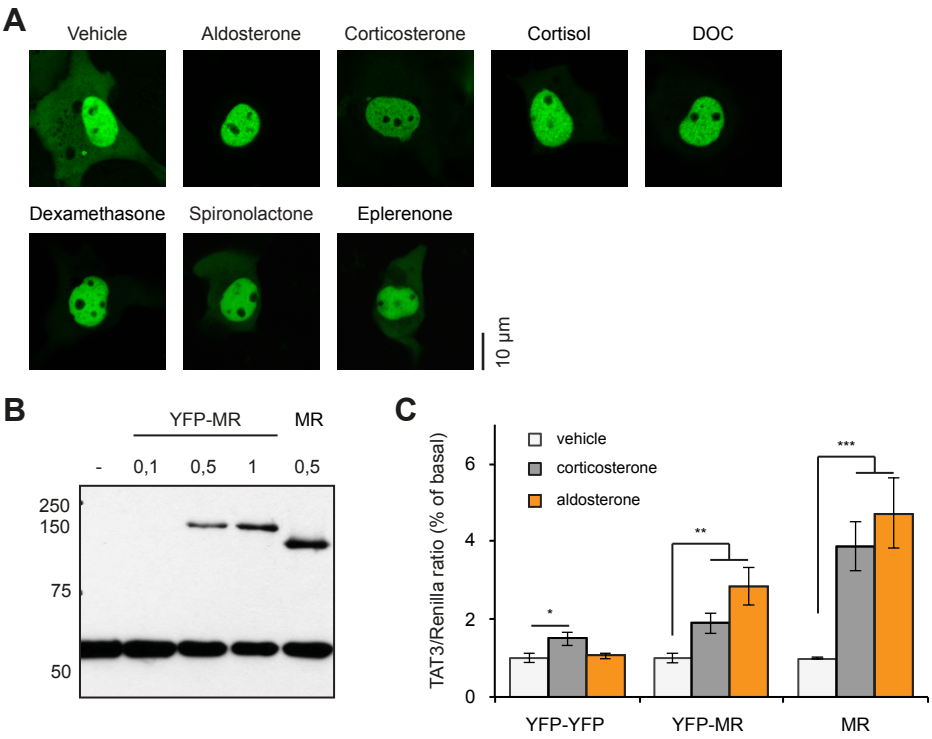

Figure 6.2: Characterization of YFP-MR
(A) Representative confocal images of YFP-MR transfected COS-1 neurons after 3 h treatment with vehicle (0.1 % EtOH) or 1 µM of hormone. YFP fluorescence was distributed over both cytoplasm and nucleus in the vehicle condition and translocated fully to the nucleus for all tested hormones. (B) COS-1 cells transfected with YFP-MR or untagged MR were analyzed on western blot and stained for MR and α-tubulin. A 60 kDa α-tubulin band was observed for all samples. MR transfected cells showed an addition band at the expected size of MR (107 kDa), while YFP-MR transfection gave a slightly larger MR band, representing the fused MR-YFP protein (134 kDa). (C) Transactivation assay. COS-1 cells were transfected with YFP-YFP, YFP-MR or untagged MR in combination with TAT_3-Firefly and CMV-renilla luciferases and analyzed for firefly and renilla luciferase luminescence. Corticosterone or aldosterone treatment (10 nM for 20 h) led to a significant increase in TAT_3-luciferase luminescence in both the MR and YFP-MR transfected cells, while only corticosterone had a small effect in YFP-YFP transfected cells. Thus, YFP-MR has transactivational capacity, although to a lesser extent as untagged MR. $n = 8, * = p < 0.05, ** = p < 0.01, *** = p < 0.001$, unpaired t-test. Scale bars: 5 µm.

detectable MR expression was seen in untransfected COS-1 cells. The YFP tag does lead to slightly reduced expression levels of MR. Finally, we assessed the transcriptional activities by cotransfection with a luciferase gene under control of a triple-GRE (TAT_3-luciferase) (van Leeuwen et al., 2011). Both YFP-MR and MR lead to a clear induction of luciferase activity with 10 nM corticosterone or aldosterone (Figure 6.2C). Control transfected cells (with YFP-YFP) showed only a small induction after corticosterone treatment, probably due to endogenous GR expression in these cells. However, the induction of TAT_3-luciferase by YFP-MR was ∼2-fold less efficacious than that with MR alone (Figure 6.2C). Concluding, we see that YFP-MR is

fully functional, although its relative expression levels and transcriptional activity are slightly reduced.

SMM analysis of agonist-activated YFP-MR

The combination of SMM and FRAP analysis has been successfully applied to study the nuclear mobility patterns of YFP-AR and YFP-GR (van Royen et al., 2014). For both steroid receptors, three distinctive fractions were identified; a single diffusing fraction and two immobilized fraction (which differed in their respective immobilization times). However, it is not to say that a similar model would best fit the nuclear dynamics of YFP-MR also. Thus, we first applied a full, unbiased analysis of the nuclear dynamics of corticosterone-bound YFP-MR. We prepared YFP-MR transfected COS-1 cells for SMM analysis 3 to 5 days after transfection. For SMM, cells are exposed to a saturating dose (1 μM) of corticosterone for 3 to 6 hours, which leads to complete nuclear translocation of YFP-MR (Figure 6.2A). Selected nuclei were photobleached until single fluorescent peaks could be distinguished (Figure 6.1A). These peaks were attributed to single YFP-MR molecules as they had comparable width and intensity as fluorescence intensity peaks derived from single EYFP molecules previously observed using the same setup (Harms et al., 2001). In our current approach, EYFP molecules were identified with a positional accuracy of ~ 40 nm in one dimension (x or y). Next, MR mobility was analyzed by analyzing image sequences with 6.25 ms and 12.5 ms time lags (Figure 6.1B) by the Particle Image Correlation Spectroscopy (PICS) analysis method (Semrau and Schmidt, 2007). PICS detects the average mean square displacement (MSD) of YFP-MR molecules for each time lag. These displacements are subsequently fitted with multiple population models. We found that, comparable to the AR and GR, the mobility of YFP-MR could best be described with a two-population model. A one-population model gave a less accurate fit (Figure 6.1C), while a three population model did not improve the fit substantially and gave inconsistent fractions over different time lags. We thus determined the relative fraction sized and mean squared displacements (MSD) of two separate fractions of YFP-MR, a 'fast' and a 'slow' fraction.

In Figure 6.3A, the size of the 'fast' fraction is plotted against the time lag. For corticosterone-bound YFP-MR the fast fraction makes up about ~ 50 % of all nuclear molecules. This percentage decreases slightly with increasing time delays. This has been reported earlier as an experimental artifact (due to fast moving molecules 'escaping' in the Z-direction) and the population distribution of the shortest time lag was shown to be a good approximation of the real distribution (van Royen et al., 2014). Using this approach, we found a 'fast' fraction of 50.7 ± 1.4 % and a 'slow' fraction of 49.3 ± 1.4 % (Figure 6.3A). Next we plotted the MSD over time for both fractions of MR molecules (Figure 6.3B). The displacement of molecules from the 'slow' fraction did not exceed our detection limit (of 0.009 μm^2) by more than 2 fold and only increases slightly over time (D_{slow} of 0.080 ± 0.005 μm^2/s). This type of diffusion befits the slow restricted movement of chromatin-bound molecules (Blainey

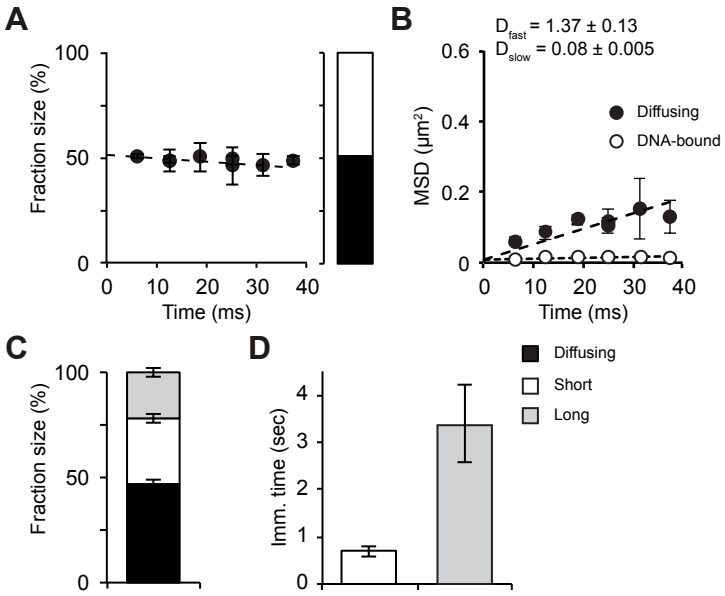

Figure 6.3: SMM and FRAP analyses provide a consistent model of the DNA-binding dynamics of agonist-bound MR
The nuclear dynamics of YFP-MR bound with corticosterone (1 μM) was analyzed by SMM (A and B) and FRAP (C and D). (A) Fraction distribution obtained with SMM. All time lags were analyzed with a two-population fit and consistently found a diffusing fraction of ∼50 %. To represent the overall fraction size the smallest time lag (6.25 ms) was used. Bar graph: diffusing fraction (black bar) and DNA-bound fraction (white bar). (B) Mean squared displacements (MSD) of both fractions in SMM. Both fractions show a linear increase in MSD over time, but with a 50-fold difference in MSD. Diffusion coefficients (D_{fast} and D_{slow}) were calculated from a linear fit of the experimental data (dashed lines; $D = \text{slope}/4$). The D_{fast} of $1.37\,\mu\text{m}^2/\text{s}$ fits to diffusing molecules, while the D_{slow} of only $0.08\,\mu\text{m}^2/\text{s}$ best fits to the slow movement of chromatin and thus DNA-bound molecules. (C) Fraction distribution obtained with FRAP. Monte Carlo simulation of corticosterone-bound MR with a 3-population model identified 3 fractions; almost half of the nuclear population is diffusing (black bar), while the remainder is subdivided into two DNA-bound fractions that differ in their immobilization times (white bar is transient bound fraction, light grey bar is more stably bound fraction). The fraction size of the diffusing fraction is similar in size as that obtained from SMM analysis. (D) Both bound fractions in FRAP are transiently immobilized, but with a 4-fold difference in duration. (A and B) Data represented as best fit ± SEM (of 3 separate PICS analyses). (C and D) Data represented as average of top 10 % best fits ± SEM.

et al., 2006; Elf et al., 2007; van Royen et al., 2014). We presume this fraction thus contains DNA-bound YFP-MR. For the 'fast' moving fraction, we saw a substantial and linear increase in displacements over time (D_{fast} of $1.37 \pm 0.13\,\mu\text{m}^2/\text{s}$), representing YFP-MR molecules diffusing freely throughout the nucleus.

Quantitative FRAP analysis of agonist-activated YFP-MR

Next, we analyzed the longer term dynamics of corticosterone-bound MR with quantitative FRAP analysis. We previously established that this technique, which uses an independent approach to quantify mobility patterns, reproduces the relative fraction sizes (of immobile and diffusing molecules) with very high accuracy

(*Chapter* 5; van Royen et al., 2014). In addition, FRAP analyzes the mobility pattern of fluorescent molecules over time frames from 100 ms up to a minute and can therefore distinguish immobilization times. As with SMM, YFP-MR transfected COS-1 cells were treated for 3–6 hours with 1 μM corticosterone. Moderately fluorescent nuclei were identified and a small strip spanning the entire nucleus was bleached with a short pulse of full laser power (Figure 6.1D). We observed that all fluorescence recovered within 30 seconds, suggesting that YFP-MR is completely mobile within this time frame (Figure 6.1D). The obtained recovery curves were quantitatively analyzed by fitting them to FRAP curves generated using Monte Carlo simulations (van Royen et al., 2009a, 2014). Diffusion rates as obtained by SMM were used as a fixed parameter in the simulations. Our data was best fitted with a model in which freely diffusing molecules show transient binding with two different durations ('short' and 'long'; Figure 6.1D).

First, we established that FRAP analysis gives a comparable fraction distribution as observed in the SMM analysis. Indeed, where SMM analysis found that 50.7 ± 1.4 % of all corticosterone-bound YFP-MR molecules were diffusing, FRAP analysis gave a 47 ± 2.1 % diffusing fraction (Figure 6.3C). Additionally, within this longer time frame, we can subdivide the immobile fraction into two immobile fractions, which differ in their immobilization time. The 53 % of immobilized molecules were further subdivided into a fraction of 31 ± 2.3 % with an immobilization time of 0.8 ± 0.1 s and a second fraction of 22 ± 2.5 % with a longer immobilization time of 3.4 ± 0.8 s (Figure 6.3D).

Taken together, we show that the combination of FRAP and SMM gives a reliable quantitative picture of YFP-MR intranuclear mobility patterns. The combination of techniques shows that upon activation by corticosterone, MR spends approximately half of the time diffusing throughout the nucleus and the other half being immobilized for short periods (0.1 to 3 seconds).

Combined SMM and FRAP analysis of antagonist-bound YFP-MR

To investigate the effect of different types of ligands on MR's nuclear mobility we first analyzed its nuclear mobility pattern when bound to an antagonist. We treated YFP-MR expressing COS-1 cells with 1 μM of two MR antagonists, spironolactone and eplerenone, and analyzed the receptor mobility by SMM and FRAP. This high dose was sufficient to induce complete nuclear translocation of the MR with both antagonists (Figure 6.2A). YFP-MR bound to either spironolactone or eplerenone remained highly mobile within the nucleus. A larger fraction of nuclear YFP-MR was diffusing: for spironolactone 78.8 ± 2.3 % to 71 ± 3.5 % and for eplerenone 68.2 ± 6.6 % to 66 ± 1.6 % and (obtained with SMM and FRAP analysis respectively; Figure 6.4A,C), which is approximately 1.5 × higher as what was observed for corticosterone-bound MR. This diffusing fraction also diffused approximately twice as fast as compared to corticosterone-bound MR (D_{fast} of 2.71 ± 0.05 and 2.49 ± 0.12 μm^2/s for spironolactone and eplerenone respectively; Figure 6.4B).

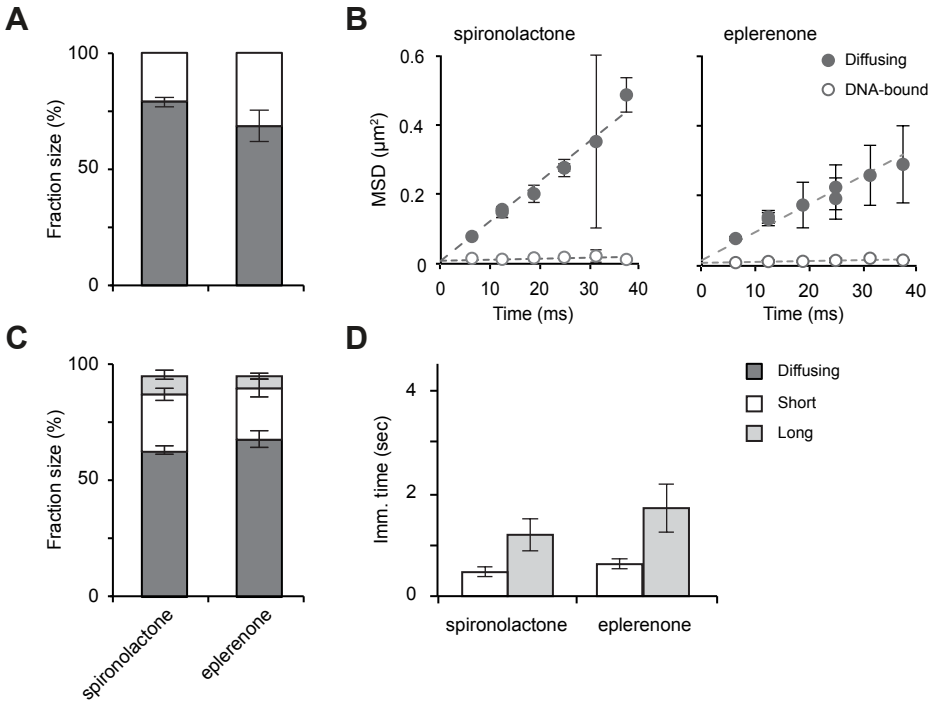

Figure 6.4: Antagonist-bound MR shows a shift towards shorter and less frequent DNA-binding
The nuclear dynamics of YFP-MR bound to its antagonists: spironolactone and eplerenone (both 1 μM) was analyzed by SMM (A and B) and FRAP (C and D). (A) Fraction distribution obtained with SMM. For all time lags a large diffusing fraction was found for both antagonists. Diffusing fraction (grey bar) and DNA-bound fraction (white bar). (B) Mean squared displacements (MSD) of both fractions in SMM. The diffusing fraction shows large displacements over time, while the DNA-bound fraction shows the small displacements expected from chromatin bound molecules. (C) Fraction distribution obtained with FRAP. Monte Carlo simulations with a 3-population model identified 3 fractions; a large diffusing fraction (grey bar), a transiently bound fraction (white bar) and a very small longer-bound fraction (light grey bar). The fraction size of the diffusing fraction is similar in size as that obtained from SMM analysis. (D) Both bound fractions are only transiently immobilized, with a 2–3 fold difference in immobilization times. (A and B) Data represented as best fit ± SEM (of 3 separate PICS analyses). (C and D) Data represented as average of top 10 % best fits ± SEM.

Finally, especially the fraction of longer DNA-binding events was much reduced for antagonist-bound MR. Spironolactone-bound MR induces a 23 ± 3.7 % fraction that is transiently immobilized (0.5 ± 0.1 sec), but has a negligible fraction of 6 ± 1.6 % that shows longer immobilizations (of 1.2 ± 0.3 sec). A similar pattern was observed for eplerenone: 25 ± 2.7 % immobilized for 0.6 ± 0.1 seconds and only 9 ± 2.3 % immobilized for 1.7 ± 0.5 seconds (Figure 6.4D). Thus, the entire population of nuclear MR is shifted towards a more mobile state with longer stretches of 'free' diffusion, a higher diffusion coefficient and fewer and shorter immobilizations.

A general pattern of intranuclear mobility after activation by different agonists

For the GR we established that a faster intranuclear mobility was seen not only for antagonist-bound receptors but also when bound to lower efficacy agonists (*Chapter 5*; Schaaf and Cidlowski, 2003). This effect was associated with multiple functional side-groups of the agonists and their interactions with specific amino acids within the ligand-binding groove of the receptor. The GR and MR share a number of (natural) agonists, but with very different relative affinities and associated differ in a number of the amino acids lining their ligand binding groove (Fagart et al., 1998; Bledsoe et al., 2005; Li et al., 2005). To assess the relationship between ligand side-groups and MR's intranuclear mobility, we tested an array of different agonists (natural and synthetic) on the mobility pattern of YFP-MR. A panel was tested that enabled us to study the effects of the P18-keto, and 11- and 17-hydroxyl groups on naturally occurring mineralocorticoid receptor agonists. We used aldosterone (which contains an 18-keto and 11-hydroxyl group), corticosterone (same structure as aldosterone, but lacking the 18-keto group), cortisol (same structure as corticosterone, but containing an additional 17-hydroxyl group), and deoxycorticosterone (DOC; same structure as corticosterone, but lacking the 11-hydroxyl group) (see Figure 6.5A). We also added the GR agonist dexamethasone, which is a weak MR agonist (Arriza et al., 1987; Hellal-Levy et al., 1999).

All ligands used induced complete nuclear translocation of YFP-MR at the high dose used (1 μM; Figure 6.2A). As compared to corticosterone, aldosterone and cortisol induced a similar mobility of the MR, which indicates that the 18-keto and 17-hydroxyl groups are not involved in determining MR's mobility (Figure 6.5 and Table 6.1). In contrast, DOC induced a higher mobility, with a 57 ± 1.5 to 60.5 ± 3.6 % diffusing fraction and smaller DNA-bound fractions (but no effect on immobilization times). This suggests that the presence of the 11-hydroxyl group results in less frequent DNA-binding. As expected, the GR agonist dexamethasone induced a very mobile receptor, intermediate between agonist- and antagonist-bound MR (Figure 6.5).

6.4 Discussion

Here we utilized a combination of SMM and FRAP to quantify the nuclear dynamics of the MR. With SMM we reliably identified two fractions of MR molecules: one that shows diffusion and one that is DNA-bound (Table 6.1). These two populations of nuclear MR molecules were found for both agonist and antagonist bound MR, but with a decrease of the fraction size of the DNA-bound molecules for antagonists. We complemented SMM with a quantitative FRAP approach, and found two bound fractions and a single diffusing fraction. The binding times of both bound fractions are orders of magnitude longer than the time scale used in our SMM experiments

		SMM		FRAP	
		Fraction size (%)	D (μm^2/s)	Fraction size (%)	Imm. time (s)
Aldosterone	Diffusing	54.1 ± 3.4	1.43 ± 0.04	45.0 ± 1.7	-
	Short	45.9 ± 3.4	0.050 ± 0.002	32.0 ± 2.0	0.8 ± 0.1
	Long			23.0 ± 2.1	2.9 ± 0.5
Corticosterone	Diffusing	50.7 ± 1.4	1.37 ± 0.13	47.0 ± 2.1	-
	Short	49.3 ± 1.4	0.080 ± 0.005	31.0 ± 2.3	0.7 ± 0.1
	Long			22.0 ± 2.5	3.4 ± 0.8
Cortisol	Diffusing	51.5 ± 0.8	1.96 ± 0.19	44.0 ± 2.2	-
	Short	48.5 ± 0.8	0.050 ± 0.002	32.0 ± 2.9	0.6 ± 0.1
	Long			24.0 ± 2.7	2.3 ± 0.3
DOC	Diffusing	60.5 ± 3.6	1.60 ± 0.13	57.0 ± 1.5	-
	Short	39.5 ± 3.6	0.060 ± 0.003	23.0 ± 3.0	0.6 ± 0.1
	Long			20.0 ± 3.1	2.3 ± 0.3
Dexamethasone	Diffusing	64.3 ± 6.0	1.74 ± 0.20	67.0 ± 2.1	-
	Short	35.7 ± 6.0	0.040 ± 0.003	22.0 ± 4.4	0.7 ± 0.1
	Long			11.0 ± 3.1	1.7 ± 0.5
Eplerenone	Diffusing	68.2 ± 6.6	2.49 ± 0.12	66.0 ± 1.6	-
	Short	31.8 ± 6.6	0.060 ± 0.004	25.0 ± 2.7	0.6 ± 0.1
	Long			9.0 ± 2.3	1.7 ± 0.5
Spironolactone	Diffusing	78.8 ± 2.3	2.71 ± 0.05	71.0 ± 3.5	-
	Short	21.2 ± 2.3	0.060 ± 0.018	23.0 ± 3.7	0.5 ± 0.1
	Long			6.0 ± 1.6	1.2 ± 0.3

Table 6.1: SMM and FRAP analyses of all MR ligands
Short, 'short' bound fraction; long, 'long' bound fraction; imm. time, average immobilization time. Results are represented as best fit ± SEM (of three separate fits) for SMM and as average ± SEM of top 10 % fits for FRAP.

and these fractions combined represent the single bound fraction detected in SMM, providing two independent estimates of the size of this (combined) fraction. Within our 7 different treatment groups, the sizes of the combined bound fractions determined by SMM and FRAP showed an average difference of only 5.2 ± 1.1 %. This high level of consistency between the two independent techniques shows that a combination of techniques generates a reliable quantitative description of protein dynamics. We have previously shown that this combination of techniques reliably assessed chromatin-binding dynamics of the GR (*Chapter 5*) and the AR (van Royen et al., 2014) as well.

We assessed the nuclear dynamics of the MR when bound to a number of natural agonists, a weak synthetic agonist and two antagonists. In general, we found that the three most potent natural agonists (aldosterone, corticosterone, and cortisol) induce a very similar pattern of nuclear MR dynamics (see Table 6.1). When bound to either of these agonists, approximately ∼50 % of all MR molecules are diffusing (with a diffusion coefficient of ∼1.5 μm^2/s) while the remaining half is DNA-bound at any time. DNA binding times range from ∼0.6 seconds (30 % of MR population)

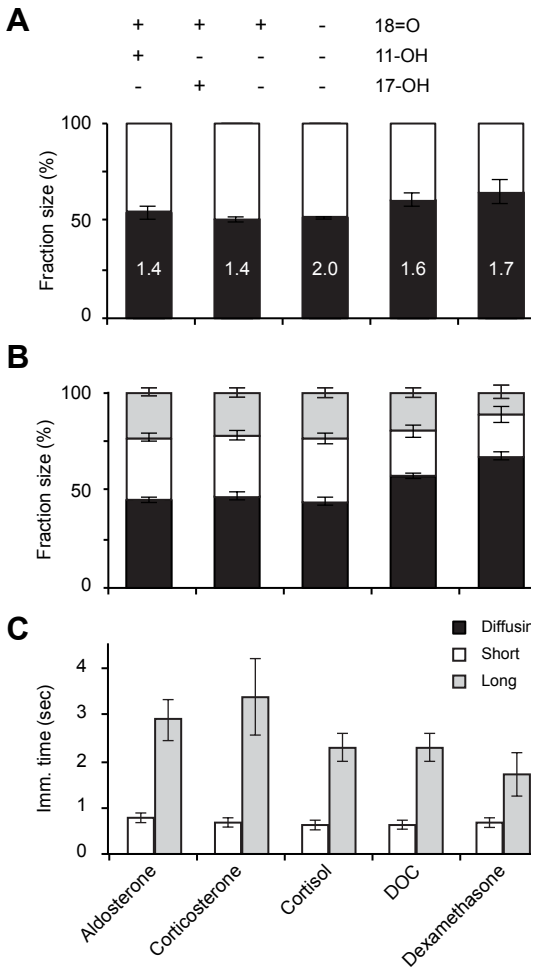

Figure 6.5: A panel of agonists identifies a structural determinant MR's DNA-binding dynamics
A range of natural agonists and one synthetic agonist were tested for their effect on the intranuclear mobility of the MR by both SMM (A) and FRAP (B-C) analysis. (A-B) Black bars represent the diffusing fraction with the diffusion coefficient written within its corresponding bar in A (in $\mu m^2/s$). White and light grey bars represent the DNA-bound fractions. (C) Immobilization times of the short-bound (white bars) and long-bound (light grey bars) fractions. With the combination of 5 agonists tested, we could examine the effect of 3 structural steroid side groups. Only for the 11-hydroxyl group (11-hydroxyl) an association with MR's DNA-binding pattern was found: DOC that lacks this group shows a lower frequency of (short) DNA-binding events. The poor MR agonist dexamethasone induced a very mobile MR with a low frequency and duration of DNA-binding events. SMM: $n = 20$, FRAP: $n = 30$. Data represented as total fit $\pm$ SEM (of 3 separate PICS analyses) for SMM and as average of top 10 % fits $\pm$ SEM for FRAP. aldo: aldosterone, cort: corticosterone, csol: cortisol, dex: dexamethasone. The data for corticosterone-bound MR is the same as in Figure 6.1.

to 2–3 seconds (20 % of MRs). When bound to an antagonist (spironolactone or eplerenone), the same three fractions still exist, but the entire population is shifted towards a more mobile and less stably (DNA-)bound MR. Under these conditions, only $\sim$30 % of all nuclear MR molecules are associated with DNA. In addition we also measured MR's DNA-binding dynamics when bound to dexamethasone, a high affinity GR agonist. Dexamethasone is known to bind with moderate affinity to the MR but has little potency for MR activation in cells (Arriza et al., 1987; Hellal-Levy et al., 1999). Associated, dexamethasone-bound MR shows high nuclear mobility, and takes up an intermediate position between the natural (highly potent) agonists and the two antagonists (Table 6.1). In most cases, the entire pattern of nuclear mobility was affected: reduced DNA-bound fractions, immobilization times and a higher effective diffusion coefficient (Table 6.1). A similar relationship between diffusion coefficients and DNA-binding frequency and duration was also seen for the

GR (*Chapter 5*). This correlation suggests that the same process, i.e. decreased DNA-binding affinity, underlies these effects. A lower effective diffusion coefficient could be obtained if very transient (< 6 ms) DNA-binding events are 'hidden' in the diffusion coefficient and the frequency of these transient events is affected by ligand properties.

The MR has long remained an understudied receptor. Few studies have assessed its nuclear dynamics (Tirard et al., 2007; Nishi et al., 2011), and none has compared different ligands. Here, we show that the MR has a similar rapid dynamics within the nucleus as seen for other steroid receptors: a combination of free diffusion and transient DNA-interactions (Stenoien et al., 2000; Rayasam et al., 2005; van Royen et al., 2014). Within the family of steroid receptors, the MR is most closely related to the GR with a high sequence homology, shared ligands and even the possibility to form MR-GR heterodimers on the DNA (Trapp et al., 1994; Liu et al., 1995; de Kloet et al., 1998). Therefore, we expected the MR to also support similar DNA-binding dynamics as the GR. Indeed, when compared to the GR and AR that were studied with the same combination of imaging techniques (van Royen et al., 2014), we find that the MR and GR display highly similar characteristics. For example, agonist-bound AR shows much longer stable DNA-binding ($\sim$8 s) than agonist-bound MR and GR (both: 2–3 s).

Mineralocorticoids and glucocorticoids do not differentially affect MR's nuclear dynamics

The MR can be bound by two functionally distinct groups of ligands, mineralocorticoids (aldosterone and DOC) and the naturally occurring glucocorticoids (cortisol and corticosterone) (Joëls et al., 2008). Brain MR binds these steroids equally well, but in the kidney MR is shielded from glucocorticoids because of enzymatic breakdown, rendering the kidney MR selective for mineralocorticoid only (Edwards et al., 1988; Funder et al., 1988). Aldosterone-bound MR is known to bind to a different set of genes (Sato and Funder, 1996; Wilson et al., 2009; Fuller et al., 2012) and was recently found to also bind to different cofactors as MR bound to endogenous glucocorticoids (Fuller et al., 2012). However, despite these differences we found no major differences in DNA-binding frequency or stability between aldosterone-bound or cortisol/corticosterone-bound MR. Thus, the subtle differences in the set of genes targeted by aldosterone-bound MR and cortisol/corticosterone-bound MR appear not to affect its overall binding profile to DNA. In addition, aldosterone has 3–4 fold slower dissociation from the MR than cortisol or corticosterone (Hellal-Levy et al., 1999, 2000), suggesting that ligand dissociation dynamics do not affect the DNA-binding dynamics of the receptor in our experiments either.

Structure-function relationship of agonist binding

For the GR, we have previously established a relationship between specific steroid side groups and the duration and frequency of DNA binding of the receptor. Most notably steroids containing the 17-hydroxyl and / or the 9-fluoro groups were shown to lead to longer and more frequent DNA-binding of the GR (*Chapter* 5). A similar relationship could be expected for the MR as well. However, as the ligand-binding pockets of the GR and MR differ in a number of key features (Fagart et al., 1998; Li et al., 2005) different functional side groups of the agonists are known to affect binding strength of the ligands to the MR (Huyet et al., 2012). Here, we tested the effects of the 18-keto (=O) and 11- and 17-hydroxyl (–OH) groups. The only side group we found to affect MR's DNA-binding dynamics was the 11-hydroxyl group. When bound to DOC, that lacks this side group, the MR shows reduced DNA-binding as compared to corticosterone, cortisol and aldosterone (all of which have the 11-hydroxyl group; Figure 6.5 & Table 6.1). Interestingly, the strongest effect was seen on the frequency of short, and not of longer, binding events. *In vitro* DOC is a selective activator of the MR, with transactivational activities that are within the same range as those of aldosterone, corticosterone and cortisol (Hellal-Levy et al., 1999; Bledsoe et al., 2002; Quinkler et al., 2002). *In vivo*, however, its potency is debated as it shows near-aldosterone potency on some MR actions (e.g. on sodium retention), but retains only limited potency on other MR actions (e.g. potassium excretion) (Vinson, 2011). That the 11-hydroxyl group is important is clearly illustrated by the fact that oxidation of this group renders cortisol and corticosterone inactive (Edwards et al., 1988; Funder et al., 1988). But, how the 11-hydroxyl group affects the ligand-receptor binding is unclear. It has not been found to undergo specific interactions within the LBP directly (Fagart et al., 1998; Auzou et al., 2000; Bledsoe et al., 2005). Another difference between binding of DOC and aldosterone/corticosterone has been found for the strength of binding to Asparagine 770 (Asn770), a key amino acid that aids in the folding of helix 12 and thereby enables exposure of the AF-2 domain (Fagart et al., 1998; Bledsoe et al., 2005). Asn770 makes two hydrogen bonds with agonist side groups for both corticosterone and aldosterone, only one with DOC and none with any of the known antagonists (Bledsoe et al., 2005; Huyet et al., 2012). Mutation of Asn770 results in an almost complete inhibition of transactivation efficacy for all agonists (Fagart et al., 1998; Bledsoe et al., 2005). Mutational studies should be undertaken to show which of the LBP amino acids are involved in the differential effect of DOC and the other steroids tested on MRs DNA-binding pattern. Thus, also for the MR a difference in its DNA-binding dynamics is correlated to a specific steroid side group, but the relationship with the interactions of ligand side-groups to the receptor seems more complicated than what we observed for the GR and its ligands.